Adsorption (2024) 30:167–183
https://doi.org/10.1007/s10450-023-00399-7

Adsorption properties of biochars obtained by KOH activation

Katarzyna Jedynak[1] · **Barbara Charmas**[2]

Received: 7 November 2022 / Revised: 7 March 2023 / Accepted: 29 June 2023 / Published online: 15 July 2023

Abstract
In this study four kinds of biochars were prepared from the KOH modified biomass. As the carbon precursors there was used the sawdust from the following trees: oak, hornbeam, apple and cherry. The physicochemical properties of the materials were characterized by the N_2 adsorption, scanning electron microscopy, thermal analysis (TG, DTG and DTA), infrared spectroscopy, and the Boehm's titration method. Moreover, pH_{pzc} (the point of zero charge) was determined. The adsorption capacity and the temperature-programmed desorption of ammonia were also studied. The obtained activated biochars were characterized by the large specific surface area (672 to 912 m^2/g) and the total pore volume (0.30 to 0.4 cm^3/g) as well as the well-developed microporous structure (85–97%). These observations were also confirmed by the SEM analysis. The maximum NH_3 adsorption capacity of the activated biochar was determined to be 3.05 mmol/g. These results prove that the sawdust of various origins is appropriate to prepare a cost-effective, environmentally friendly biochar.

Keywords Sawdust · Biochars · KOH activation · Physicochemical properties · Adsorption · Ammonia gas

1 Introduction

In the last dozen or so years the research on biochar production was intensified. The growing interest in this material results from its numerous advantages: this is the material rich in carbon, with a large degree of porosity, large specific surface area with a stable structure, a large content of surface functional groups and a great cation exchange capacity [1–3]. In addition, biochar has a wide range of applications: agriculture—soil improvement [4],environmental protection—removal of harmful gases, i.e., CO_2, H_2S [5], NH_3 [6, 7],contaminants from the aqueous solutions—pharmaceuticals [8], dyes ([9], pesticides [10], in soil remediation from inorganic and organic pollutants [11],in energy recovery technologies—renewable fuel, catalysts [12].

Biochar can be obtained in the pyrolysis process in the inert atmosphere from virtually any type of biomass, which makes it a competitive material, much cheaper compared to the commercial materials [1, 6, 13, 14]. Besides the carbon adsorbent, there are obtained also other products such as: oil and synthesis gas. The percentage of the obtained products depends on the heating rate, temperature and pressure used during the pyrolysis [13, 15]. The precursors used to obtain biochar are e.g. wood biomass: sawdust [16, 17], cones [18–20], food or agricultural waste: nut shells [21, 22], cereal straw [1], cotton stalks [23], corn cobs [24, 25], rice husks [26], banana peels [27], coffee spent grains [28],natural fertilizers: chicken manure [29] and waste paper [30].

The adsorption properties of biochar could be improved due to development of its porosity, e.g. as a result of physical or chemical activation. Physical activation includes two stages: carbonization of the carbon precursor in the inert gas atmosphere and activation at a high temperature with the use of an oxidizing gas—carbon dioxide, steam, air or a mixture of CO_2 and steam [31, 32]). The chemical activation can take place in two ways. The first method of activation includes the carbon precursor impregnation with a chemical activator, followed by heating at an elevated temperature (carbonization/activation) [33]. The other one includes two stages. After the initial carbonization of the carbon precursor (300 to 600 °C), the biochar is impregnated with a chemical agent and then activated (700 to 1200 °C) [33].

The chemical activation is more agvantageous than the physical one due to its greater efficiency, larger surface areas and the more developed porous structure of the obtained

✉ Katarzyna Jedynak
kjedynak@ujk.edu.pl

[1] Institute of Chemistry, Jan Kochanowski University, 25-406 Kielce, Poland

[2] Institute of Chemical Sciences, Faculty of Chemistry, Maria Curie-Sklodowska University, 20-031 Lublin, Poland

materials [34]. The use of the activation process with KOH as an activating agent leads to the formation of a well-developed porous structure on the biochar surface with a predominance of micropores as well as the appearance of active functional groups [35, 36]. It was proved that the content of micropores on the surface of active carbon increases slightly with the increasing extent of impregnation [37]. This is due to a more intensive reaction between the KOH and carbon surface which results in a greater release of CO_2 and CO gases as well as the micropores formation [38]. Zhu et al. [39] obtained a biochar with a large specific surface area (782–2435 m^2/g) and developed microporosity (0.301–0.625 cm^3/g) using the Paulownia sawdust as a carbon precursor. The raw sawdust was preheated in the oven (250 °C, 2 h, N_2), then the material was impregnated with KOH (80 °C, 12 h) and the activation process took place. There were used the following conditions: impregnation KOH/C weight ratio 2:1, 4:1 and 6:1; activation temperatures 600, 700, 800 and 900 °C; activation time 0.5, 1 and 2 h. In turn, Yang et al. [40] obtained structured porous biocarbons in the two-stage process involving hydrothermal treatment and carbonization of the Cedar wood sawdust. The dried sawdust (105 °C, 24 h) was poured with the 5 wt% KOH solution and subjected to the hydrothermal treatment (the bottle hermetically closed with a lid, the temperature 120 °C, for: 30 min, 2 h and 8 h). After the hydrothermal treatment, the suspension was separated by filtration and dried at 105 °C until the stable weight. The obtained product was carbonized (800 °C, 5 °C/min, 1.5 h) in the argon atmosphere. The activated biochars were characterized by the following parameters: specific surface area (875–908 m^2/g), volume of micropores (0.406–0.420 cm^3/g). Quan et al. [41] obtained a biochar from the pine sawdust. The pyrolysis was performed at 700 °C (temperature increase 10 °C/min) for 2 h. Then the activation was made with KOH. After the pyrolysis the biochar was mixed with KOH at the weight ratio of 4:1, placed in the boats in the tube furnace, and the activation was performed at the temperatures of 700, 800, 900 °C for 2 h in the nitrogen atmosphere. The obtained materials were characterized by the large specific surface area $S_{BET} = 1729 - 2331$ m^2/g and the volume of micropores $V_{mi} = 0.671 - 0.795$ cm^3/g. Liu et al. [42] used the coconut shell as the biochar precursor. The crude material was impregnated with the KOH solution followed by activation at 700 °C. The obtained biochar had the developed microporous structure ($V_{mi} = 0.315$ cm^3/g) and the large specific surface area (860 m^2/g). Marques et al. [43] obtained the apple tree small branches biochar impregnated with the KOH solution and then activated at 800 ℃ (1–4 h). The finally obtained biochars were characterized by the large specific surface (2114–2472 m^2/g) and the developed microporosity (91–98%). Oginni et al. [33] compared the biochars obtained from two types of biomass: Kanlow Switchgrass (KS) and Public Miscanthus (PM) as a result of one and two-stage activation. The raw biomass was heated at 500 °C. Then the starting biomass and the biochar after the pyrolysis were impregnated with KOH at the weight ratio of 1:1. The activation of the materials obtained by these methods was performed at 900 °C for 0.5 h. The specific surface area values were higher for the materials obtained as a result of raw biomass impregnation (one-step activation). The S_{BET} values differed depending on the precursor and the method of preparation (KS: 599–1272 m^2/g and PM: 957–1597 m^2/g). Applying various carbon precursors and two different methods (carbonization-activation and impregnation-activation) at two different KOH/carbon ratios Elmouwahidi et al. [44] obtained materials with a developed porosity. To sum up, the porous structure and properties of the ultimately obtained biochars depend on both the nature of the starting material and to a large extent on the parameters of the activation process [45].

Toxic gases that pollute the environment pose a serious threat to human health [46]. One of these gases is ammonia. Right after dinitrogen oxide (N_2O), this gas is one of the most common compounds in the atmosphere [46, 47]. Ammonia is a poisonous gas which is also a valuable chemical raw material used in industry, among others, for the production of varnishes, plastics, rubbers, disinfectants, battery-killing agents, fertilizers and in cooling installations as a cooling gas [48, 49]. When the content of ammonia in the atmosphere exceeds 35 ppm, it has a negative effect on human and animal health [50]. Therefore, for the sake of the safety of the natural environment and people, it is very important to eliminate this gas from the surrounding atmosphere.

One of the most frequently used methods of removing ammonia polluting the air, taking into account the low cost, simplicity of implementation and efficiency in a wide range of concentrations, are adsorption processes [51]. The adsorbents that work best during this process should have a well-developed surface and porosity, which will ensure great ammonia removal capacity [49].

The aim of the paper was to obtain a biochar with developed porosity from the low-cost KOH-activated sawdust and to investigate the influence of the type of carbon precursor on the physicochemical and sorption properties against the gas phase impurities represented by ammonia. To sum up, it was crucial for us to obtain effective adsorbents with a great adsorption capacity for removal of ammonia and possibly in the future of other toxic gases from the air, e.g. nitrogen oxides NO_x, sulfur oxides: SO_2 and SO_3 as well as carbon oxides: CO and CO_2.

2 Experimental

2.1 Chemicals

The ultra-high purity (UHP) nitrogen 5.0 (99.999%) for preparation of biochars was purchased from Air Liquide (5.0), Poland. Potassium hydroxide for activation of the porous structure of biochars was purchased from POCh, Poland.

The gases, UHP helium 5.0 (99.999%) for cleaning (stabilization) of biochar and temperature-programmed desorption of ammonia (TPD), and UHP 10% ammonia in helium for the pulse chemisorption were purchased from Air Liquide, Poland.

2.2 Materials

The sawdust used as the carbon precursors was obtained from the treatment of the following deciduous trees: oak, hornbeam, cherry and apple. The raw sawdust was ground in the laboratory mill (MF 10, IKA, Germany) to collect the grain size fraction smaller than 2 mm. Then the materials were placed in the quartz boats and heated in the tube furnace (MRT-4, Czylok, Poland) to 800 °C at the heating rate of 2 °C/min with the additional isothermal stages at 180 °C (2 h), 400 °C (2 h) and the final temperature 800 °C (3 h). The process proceeded in the nitrogen atmosphere at the gas flow rate of 20 dm^3/h. The obtained biochars were designated C–O (Carbon–Oak), C–H (Carbon–Hornbeam), C–A (Carbon–Apple) and C–C (Carbon–Cherry).

For developing develop the porous structure of the obtained biochars, the activation process was conducted. The obtained materials were mixed with KOH at the weight ratio of 1:2 and 1:4 (biochar:KOH), then placed in the quartz boats and annealed (5 °C/min) in the tube furnace to 600 °C at the nitrogen flow rate of 20 dm^3/h. The materials were soaked at 600 °C for 2 h. The obtained materials were designated $C–O_{1\text{-}2}$, $C–H_{1\text{-}2}$, $C–A_{1\text{-}2}$, $C–C_{1\text{-}2}$ and $C–O_{1\text{-}4}$, $C–H_{1\text{-}4}$, $C–A_{1\text{-}4}$, $C–C_{1\text{-}4}$.

2.3 Characterization

The low-temperature nitrogen adsorption/desorption isotherms were measured at 77 K using the ASAP 2020 volumetric analyzer (Micromeritics Inc., Norcross, GA, USA) in the Structural Research Laboratory at Jan Kochanowski University in Kielce. Just before the measurements, all samples were degassed at 200 °C for at least 2 h.

Scanning electron microscopy images were obtained using the scanning electron microscope (SEM Zeiss Ultra Plus, EDS Bruker Quantax 400, Germany). During the measurements the voltage of 2 kV was applied. The energy-dispersive X-ray spectroscopy (SEM/EDX, acceleration: 15 kV) was used for the quantitative measurements.

The Perkin–Elmer Spectrum 400 FT-IR/FT-NIR spectrometer (Perkin–Elmer, Waltham, MA, USA) with the endurance single bounce diamond, attenuated total reflection (ATR) cell was used for spectra registration. The spectra 4000–650 cm^{-1} were recorded. All materials were dried and ground before the measurements.

The Boehm's titration method [52, 53] was used for determination of the functional acidic and basic oxygen surface groups. The 0.2 g mass weights of the biochars were dispersed in the sodium bicarbonate, sodium carbonate, sodium hydroxide and sodium ethoxide solutions (all at the concentration of 0.1 mol/dm^3) for determination of the functional acidic groups. However, hydrochloric acid (0.05 mol/dm^3) was used for determination of the total basic groups. After shaking for 48 h at room temperature the suspensions were filtrated and 10 cm^3 of the filtrate was titrated with 0.1 mol/dm^3 HCl for determination of the acidic groups and with 0.05 mol/dm^3 NaOH for the total basic group determination. The titration endpoint was determined using the methyl orange indicator.

The biochars pH_{pzc} (point of zero charge) was analyzed by means of the method used in [54, 55]. At the beginning the solutions of the pH between 3 and 12 in the 0.01 mol/dm^3 NaCl solution were prepared by adding 0.1 or 1 mol/dm^3 of HCl and 0.1 or 1 mol/dm^3 of NaOH. The biochar samples (0.15 g) were added to the solutions (50 cm^3) with an appropriate pH value. Next, they were shaken in the incubator (Orbital Shaker-Incubator ES-20, Grant-bio) for 180 min at 298 K. Then the final pH was measured. After this time, the relationships between the final and the initial values of pH were determined. The pH_{pzc} indicates the intersection point of the experimental curves and $pH_{initial} = pH_{final}$ line [54, 55]. The pH-meter inoLab pH 730, WTW was used for the pH value measurement.

The thermal behavior and composition of the volatile and fixed carbon in the biochars were determined using the Derivatograph C (Paulik, Paulik & Erdey, MOM, Budapest). The tested materials (about 20 mg) were placed in the small corundum crucible. Al_2O_3 was used as the reference material. The analyses were made in air (O_2) or inert (N2) atmosphere in the temperature range from 20 to 1200 °C (heating rate 10 °C/min). The TG, DTG and DTA curves were registered.

The content of volatile carbon, i.e., less humified organic matter (%VC) was determined from the TGA data in the N_2 atmosphere in the temperature range 150–900 °C ($TG\%_{900,N2}$), assuming that the physically bound water (moisture) is desorbed up to 150 °C. The ash percentage (%A) is the residue after the complete thermal degradation of the material in the O_2 atmosphere at 1200 °C (TG%

$_{1200,O2}$). The content of fixed carbon, more humified organic matter (%FC) was determined as the difference of TG% $_{1200,O2}$ and TG% $_{900,N2}$. The share of the thermostable biochar fraction (C_{thermo}, poorly thermodegradable, ash-free, in relation to the dry mass) was also determined as the content of stable substances (%FC) in relation to the sum of volatile (%VC) and fixed substances (% FC) [56] This parameter is considered reliable for assessing the level of organic matter stability in pyrocarbons, compost materials or other organic wastes [57].

The pulse chemisorption and temperature-programmed desorption (TPD) measurements of ammonia were made using the automatic AutoChem II 2920 analyzer (Micromeritics, Norcross, GA, USA). Before testing all biochars were degassed at 200 °C for 2 h (ASAP 2020, Micromeritics, Norcross, GA, USA). The first stage of the measurements was the stabilization of the material (50 mg of biochar in the quartz reactor) in the helium atmosphere at the temperature of 250 °C (20 °C/min for 40 min).

The chemisorption studies were carried out at the three temperatures: 0 °C, 10 °C and 20 °C. The standard gas (10% NH_3 in helium) was dosed from the loop of known volume. The TCD detector registered the next doses. Dosing was performed until the surface of the analyzed material was saturated. The total amount of gaseous ammonia adsorbed on the biochar surface was calculated. In the next stage the experiments of thermo-programmed desorption were performed. The temperature increased from the measurement temperature, at which the chemisorption process was initially conducted to 250 °C (with the temperature increase rate of 10 °C/min).

2.4 Calculations

The porous structure standard parameters: specific surface area, pore volume as well as pore size distribution were determined based on the experimental nitrogen adsorption isotherms. Determination of the specific surface area (S_{BET}) was made in the range of the relative pressure from 0.05 to 0.20 taking into account the nitrogen molecule surface area equal to 0.162 nm^2 [58]. Determination of the total pore volume (V_t) was made from one point of the adsorption isotherm at the relative pressure $p/p_0 = 0.99$ [59]. To calculate the pore size distribution functions (PSDs), the non-local density functional (NLDFT) method was applied for the carbon slit-shaped pores which characterizes the surface energetical heterogeneity and geometrical corrugation [60, 61]. The calculations were made applying the numerical program SAIEUS (Micromeritics). The maxima of the PSD curves were used to determine the micropore widths, w_{mi}. Microporosity, expressed in % was calculated as the ratio of the micropore volume V_{mi} to the total pore volume V_t.

3 Results and discussion

The main factors influencing the structural and surface properties of carbon materials obtained from the industrial waste are: (1) the nature of the carbon precursor, its composition and structure; (2) activation method, type and amount of activating substance. In the presented research the source of the organic matter was the sawdust of four different kinds of trees: oak, hornbeam, apple and cherry. Despite the fact that they are different species of trees, their structure was not significantly diversified. Figure 1a and b presents the experimental nitrogen adsorption–desorption isotherms for the studied biochars. All isotherms are Type I according to the IUPAC classification [62]. The large adsorption values at low relative pressures indicate a strongly developed structure of micropores in the tested materials. The almost parallel course of the isotherms to the axis of relative pressures in the range of medium and high pressures ($p/p_0 \sim 0.2–0.9$) is confirmed by a very small share of mesopores.

The lowest situated isotherms determined for the non-activated C–O and C–H biochars (Fig. 1a) as well as C–A and C–C (Fig. 1b) indicate their least developed surface and porosity. The use of KOH as an activating agent resulted in intensive development of the surface and structure of the pores, especially in the area of micropores. The influence of the amount of the activating agent is also clearly visible on the isotherms (Fig. 1). The isotherms determined for the materials with the maximum KOH content (1:4) are the highest situated, indicating the most effective development of the surface and volume of micropores. These observations are confirmed by the values of the structural parameters in Table 1.

The specific surface area (S_{BET}) values for the unactivated biochars ranged from 333 m^2/g for the C–O material to 387 m^2/g for the C–C material while the values of the total pore volume (V_t) ranged from 0.16 cm^3/g for C–O to 0.21 cm^3/g for C–C. The activation with KOH has brought very good results. The activation by mixing carbon with KOH at the ratio 1:2 resulted in the over twofold increase in the specific surface area and V_t value. For all materials obtained in this way, the surface values ranged from 714 m^2/g for the $C–O_{1-2}$ material to 788 m^2/g for the $C–C_{1-2}$ material, while the V_t values ranged from 0.33 cm^3/g for $C–O_{1-2}$ to 0.40 cm^3/g for $C–A_{1-2}$. On the other hand, the activation by mixing carbon with KOH at the ratio 1:4 improved these parameters. The values increased and ranged from 718 m^2/g for the $C–H_{1-4}$ material to 912 m^2/g for the $C–A_{1-4}$ material. The V_t values ranged from 0.33 cm^3/g for the $C–H_{1-4}$ material to 0.43 cm^3/g for the $C–A_{1-4}$ material. As the aim of these studies was to obtain a biochar with well-developed microporosity, the volumes

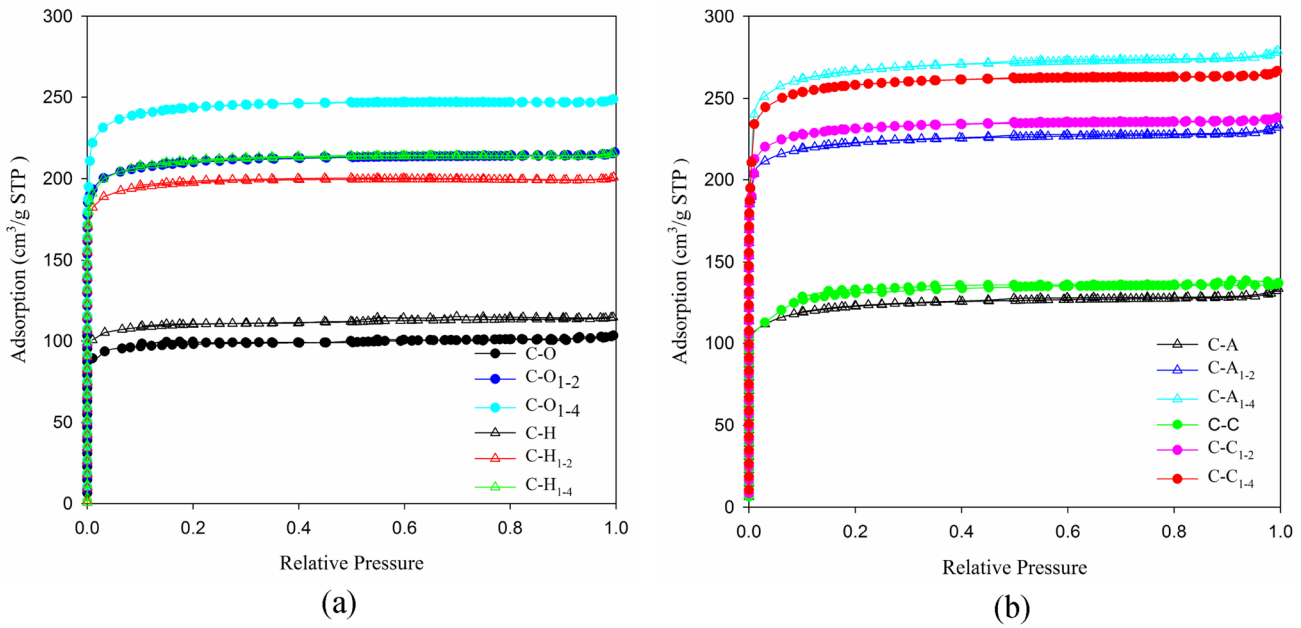

Fig. 1 Nitrogen adsorption–desorption isotherms for the biochars obtained based on the carbon precursors: oak and hornbeam sawdust (**a**) as well as apple tree and cherry tree sawdust (**b**)

Table 1 Structural parameters of the biochars

Biochars	S_{BET} (m^2/g)	V_t (cm^3/g)	$V_{ultraDFT}$ (cm^3/g)	$V_{microDFT}$ (cm^3/g)	w_{miDFT} (nm)	Micr-oporos-ity (%)
C–O	333	0.16	0.06	0.15	0.65	94
$C–O_{1-2}$	714	0.33	0.19	0.32	0.60	97
$C–O_{1-4}$	831	0.38	0.21	0.37	0.60	97
C–H	374	0.18	0.08	0.17	0.64	94
$C–H_{1-2}$	672	0.31	0.17	0.30	0.60	97
$C–H_{1-4}$	718	0.33	0.17	0.32	0.61	97
C–A	379	0.21	0.19	0.20	0.55	95
$C–A_{1-2}$	775	0.40	0.18	0.34	0.61	85
$C–A_{1-4}$	912	0.43	0.18	0.40	0.64	93
C–C	387	0.21	0.20	0.21	0.56	100
$C–C_{1-2}$	788	0.37	0.21	0.35	0.60	95
$C–C_{1-4}$	880	0.41	0.20	0.39	0.61	95

Notation: S_{BET} the BET specific surface area, V_t the pore volume, $V_{ultraDFT}$ the ultramicropores volume (pores width < 0.7 nm) obtained by the DFT method, $V_{microDFT}$ the micropores volume (pores width < 2 nm) obtained by the DFT method; obtained from the difference of V_t and V_{mi}, w_{miDFT} micropore diameter at the maximum of the PSD curve obtained by the DFT method, *Microporosity* the micropores share;

of micropores (V_{mi}) should be dominant. Our goal has been achieved. The micropore volumes determined for the materials with the most developed porosity, i.e., $C–H_{1-4}$ and $C–A_{1-4}$, are 0.32 cm^3/g and 0.40 cm^3/g, respectively. A large proportion of the micropores: from 85 to 97% was observed for all activated biochars (Table 1). It was proved that the biochar/KOH mass ratio plays an important role in the development of the porous structure. The development of the porous structure takes place as a result of the intercalation of metal (potassium) into the carbon structure and it is the larger the greater the impregnation factor is, owing to which there is formed a larger number of pores. The general reaction is as follows:

$$4\,KOH + C \rightarrow K_2CO_3 + K_2O + 2\,H_2, \quad (1)$$

however, after [63] it runs multi -stage according to the reactions:

$$2\ KOH \rightarrow K_2O + H_2O; \quad (2)$$

$$C + H_2O \rightarrow H_2 + CO; \quad (3)$$

$$CO + H_2O \rightarrow H_2 + CO_2; \quad (4)$$

$$K_2O + CO_2 \rightarrow K_2CO_3. \quad (5)$$

Moreover, if the temperature or contact time is too high or the optimal KOH content is exceeded, the activation yield decreases, pore sizes get larger and the micropores share is reduced. Then too intensive reaction of KOH with carbon takes place, causing significant losses of carbon matter. Moreover, as a result of the decomposition of an excessive amount of KOH in the system, the water is formed (reaction 2) [64, 65]. At the high temperature of the process, the water causes the excessive carbon gasification [45].

The selection of the carbon precursor plays also an important role in the development of the porous structure. The sawdust has a tubular structure [45, 66]. This type of structure, existing in the raw sawdust, allows them to adsorb effectively the reagent thus enabling the biochar activation [45].

The pore size distribution functions (PSDs) for the biochars were calculated using the DFT method. They are presented in Fig. 2a and b.

The maximum can be seen on all PSD curves, indicating the presence of pores of the sizes < 2 nm, which corresponds to the width of micropores. As follows from Table 1 the micropore sizes range from 0.55 to 0.65 nm in the case of the non-activated biochars while in the case of the materials after the KOH activation process the values vary from 0.60 to 0.64 nm.

In order to analyze the morphology of the tested biochars before and after the activation with KOH, SEM imaging was performed (Figs. 3, 4).

As follows from Figs. 3 and 4 depending on the carbon precursor the analyzed carbon materials are characterized by different porous structures. The unactivated biochars obtained based on the oak (C–O, Fig. 3a) and horn (C–H, Fig. 3d) have poorly developed porous structures. The carbons C–A (Fig. 4a) and C–C (Fig. 4d) were characterized by slightly better developed porosity in the case of the non-activated materials which was confirmed by the SEM images. It can be clearly visible that the activation with KOH caused the development of porosity of the tested biochars (Figs. 3b, c, e, f, 4b, c, e, f). In all cases after the KOH activation there was observed a layered structure which can indicate the order of the tested biochars. To sum up, it can be stated that the KOH activation affects the microporous structure of the obtained carbons including the size and volume of micropores but it does not affect mesoporosity (Table 1).

The EDS (X-ray energy dispersion spectroscopy) studies were carried out simultaneously with the SEM analysis. This technique makes the qualitative and quantitative elemental

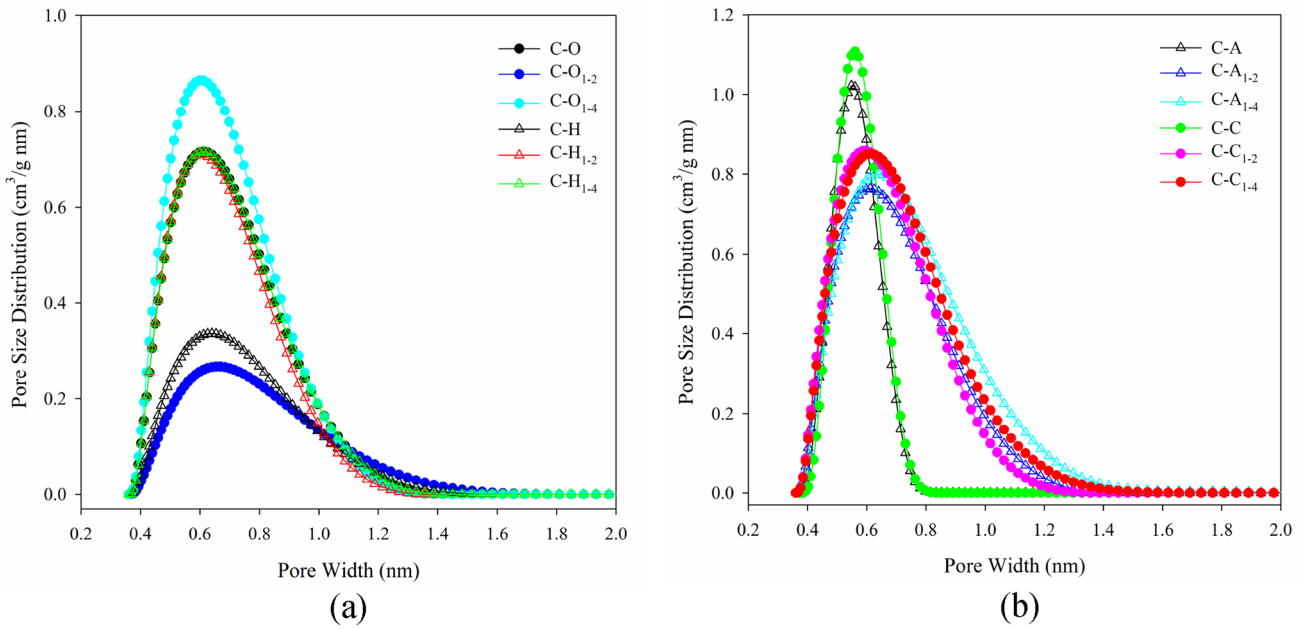

Fig. 2 Pore size distributions (PSDs) calculated by the DFT method for the biochars obtained based on the carbon precursors: oak and hornbeam sawdust (**a**) as well as apple tree and cherry tree sawdust (**b**)

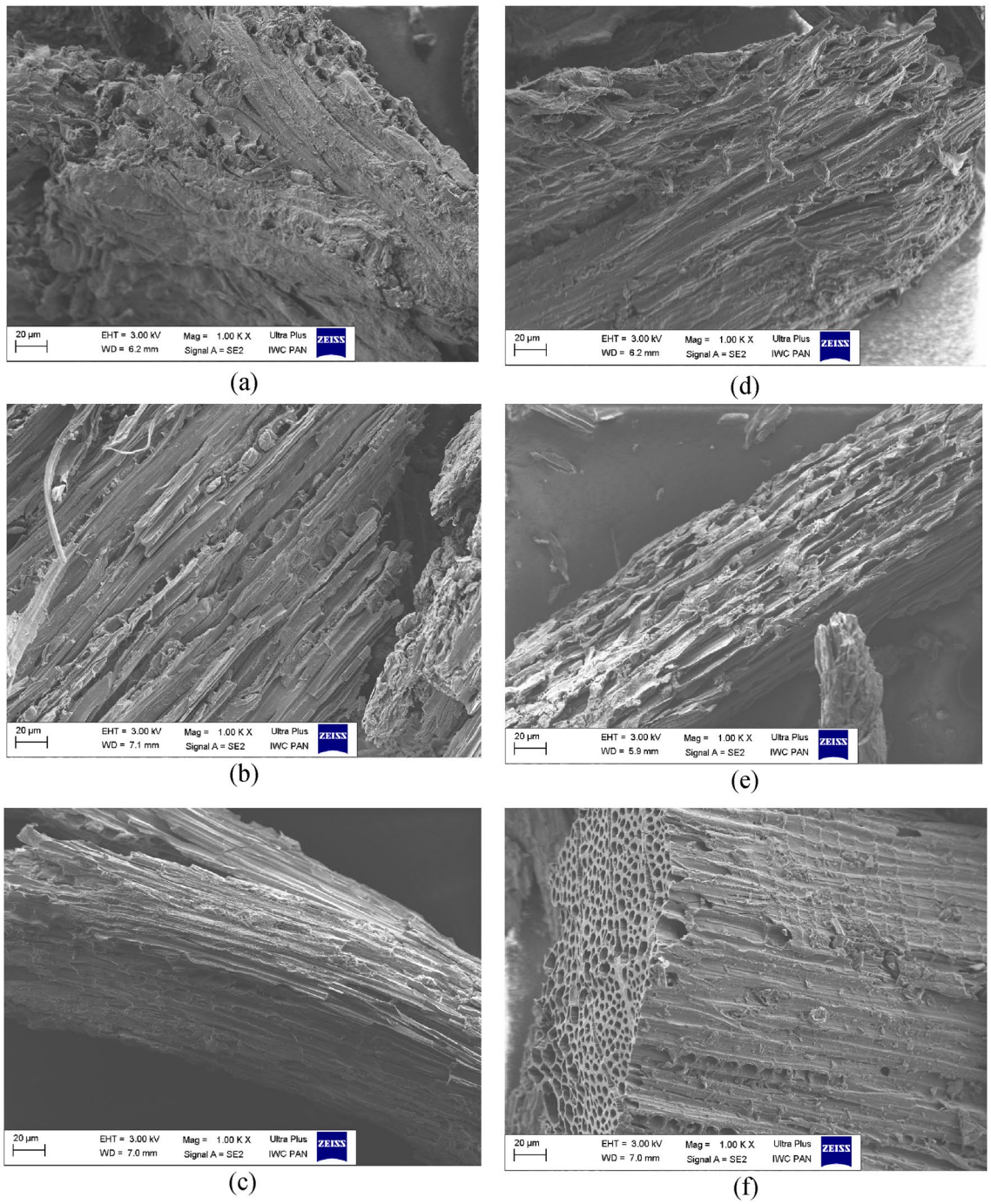

Fig. 3 SEM images for the biochars: C–O (**a**), C–$O_{1\text{-}2}$ (**b**), C–$O_{1\text{-}4}$ (**c**) and C–H (**d**), C–$H_{1\text{-}2}$ (**e**), C–$H_{1\text{-}4}$ (**f**)

analyses of the biochars possible [67]. Table 2 presents the results of EDS chemical composition microanalysis for the non-activated and KOH activated biochars.

Analyzing the obtained EDS results it can be observed that the basic chemical components of all tested biochars are carbon and oxygen and, to a much smaller extent, potassium. Only in the case of the biochar obtained from the sawdust of fruit trees, i.e., apple and cherry trees, the presence of calcium ions was additionally found. The presence of carbon and oxygen results from the presence of cellulose, hemicellulose and lignin in the wood biomass as well as in the obtained biocarbons [68, 69]. The amount of carbon in the non-activated materials ranges from 85.50 to 90.86% w/w. After the biochar activation the values are slightly smaller and range from 72.02 to 84.03%. The oxygen content is from 8.74 to 12.06% and from 13.94 to

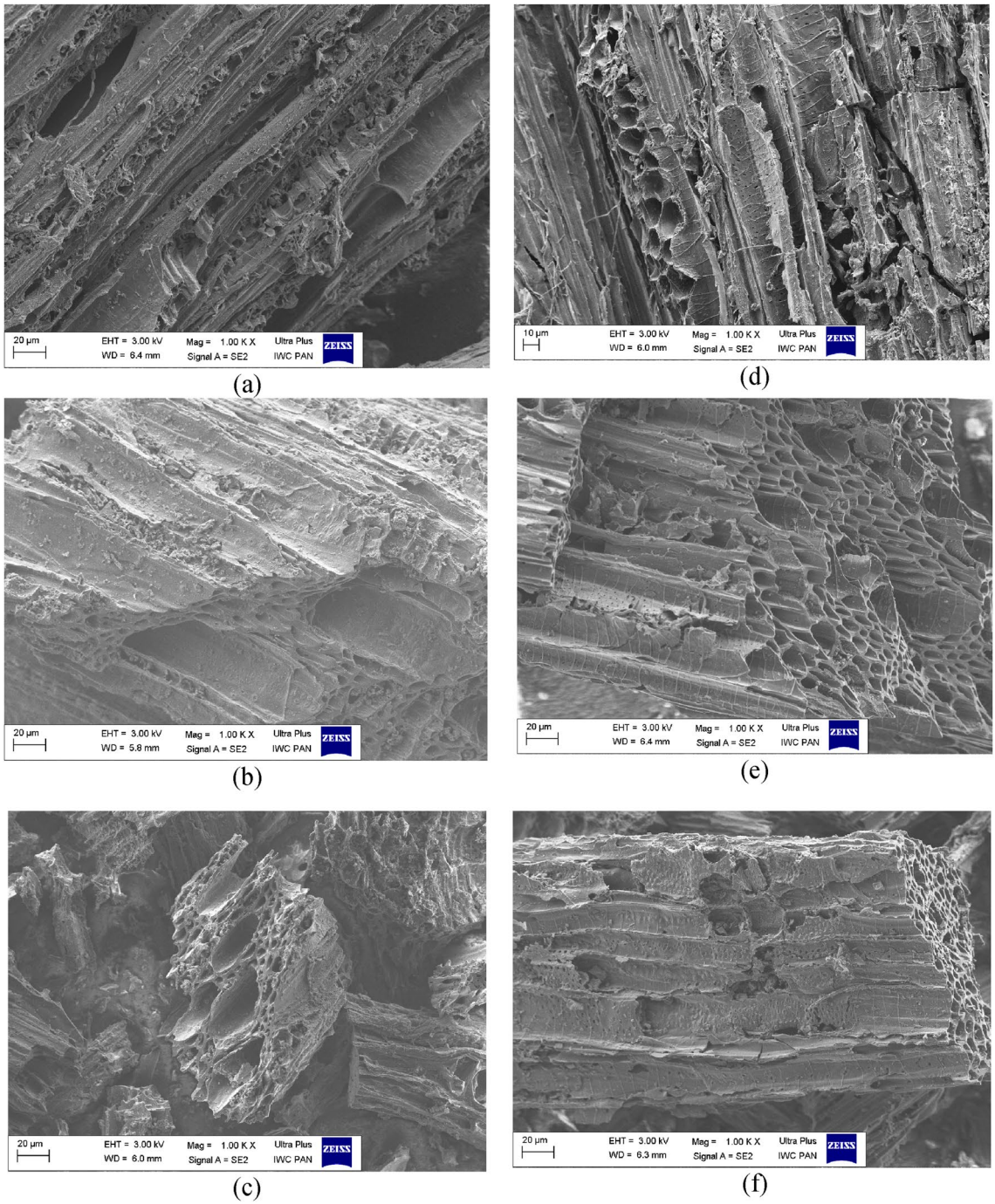

Fig. 4 SEM images for the biochars: C–A (**a**), C–A_{1-2} (**b**), C–A_{1-4} (**c**) and C–C (**d**), C–C_{1-2} (**e**), C–C_{1-4} (**f**)

22.19% for the inactivated and activated biochars, respectively. This element is bound in the form of surface oxygen groups, and the increase in its content along with that in the degree of impregnation indicates an increase in the number of these groups on the surface of the tested materials. The presence of other elements, such as potassium and calcium, is largely influenced by the chemical composition of the biomass, i.e., raw sawdust.

The presence of the surface functional groups was confirmed by the ATR-FTIR analysis (Figs. 5, 6).

The low-intensity bands in the range of 3755–3576 cm^{-1} for all analyzed materials correspond to the asymmetric

Table 2 The EDS analysis for the biochars

Biochars	C (% w/w)	O (% w/w)	K (% w/w)	Ca (% w/w)
C–O	90.86	8.74	0.40	–
$C–O_{1-2}$	82.51	16.29	1.19	–
$C–O_{1-4}$	79.32	19.26	1.42	–
C–H	90.28	9.60	0.12	–
$C–H_{1-2}$	81.59	15.34	3.07	–
$C–H_{1-4}$	80.41	15.77	3.82	–
C–A	87.81	10.34	0.80	1.05
$C–A_{1-2}$	82.93	15.78	0.09	1.20
$C–A_{1-4}$	82.07	19.43	0.01	1.54
C–C	85.50	12.06	1.01	1.43
$C–C_{1-2}$	84.93	13.94	0.13	1.00
$C–C_{1-4}$	75.02	22.19	0.20	2.59

and symmetric stretching vibrations of the surface O–H groups [20, 70–72]). In turn, the 2174 cm^{-1} band is related to the presence of carbon monoxide (CO) in the tested materials [70]. The vibrations associated with the presence of double bonds between carbon atoms or those of carbon and oxygen are responsible for the intense band at 1740 cm^{-1} [73, 74]. The band at 1570 cm^{-1} is characteristic of the C=C bond [75]. On the other hand, the bands in the range of 1500–1100 cm^{-1} (exactly at 1366 cm^{-1}, 1232 cm^{-1}, 1100 cm^{-1}) indicate the presence of carbonyl groups (C=O) [76]. Their presence on the biochar surface is consistent with the results of the Boehm titration (Table 3). In turn, the 1000 cm^{-1} and 1005 cm^{-1} bands are characteristic of the C–OH stretching vibrations [76]. The band in the range from 900 to 750 cm^{-1} indicates the C–H bending vibrations [72]. It should be highlighted that activation changes the chemical structure of the biocarbons surface. The band 1570 cm^{-1} increases with the increasing KOH ratio, while the bands at 1740, 1366 and 1232 cm^{-1} increase at the 1–2 ratio but decrease at the 1–4 KOH ratio.

The Boehm's titration method [52, 53] was used to characterize the chemical nature of biochars surface. The individual acid groups undergo neutralization in the following order: carboxylic – neutralized when influenced by $NaHCO_3$; carboxyl + lactone – affected by Na_2CO_3; carboxylic + lactone + phenolic—neutralized by NaOH; carboxylic + lactone + phenolic + carbonyl – neutralized when influenced by C_2H_5ONa. Summing up, the content of basic functionalities was determined by titration of unreacted HCl that was previously used to neutralize the basic groups using the NaOH solution. The surface functional groups have a significant impact on the adsorption process, ensuring selectivity in the removal of specific pollutants. The functional groups affect the surface charge of the adsorbent and thus its adsorption capacity [77].

The content of the functional groups determined on the surface of the studied KOH activated biochars are presented in Table 3.

The obtained results indicate the predominance of acidic and basic groups on the surface of the tested biochars. Note that an increase in the KOH ratio results in an increase mainly in the carboxyl and carbonyl groups and to a much smaller extent in the phenolic ones, which is consistent with the pH_{pzc} data. As can be seen, the number of functional

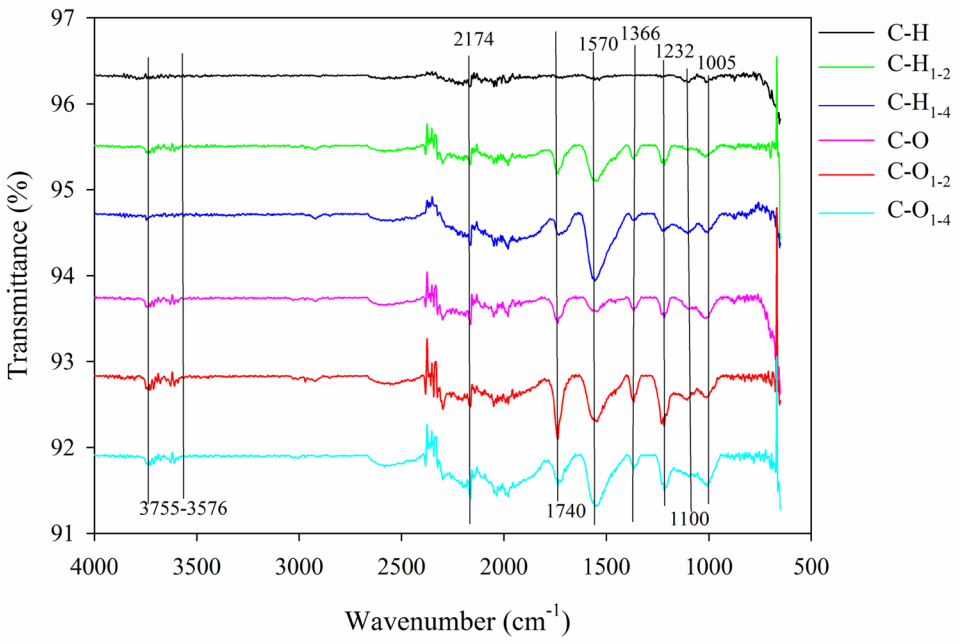

Fig. 5 FTIR spectra for the biochars obtained from the hornbeam and oak sawdust

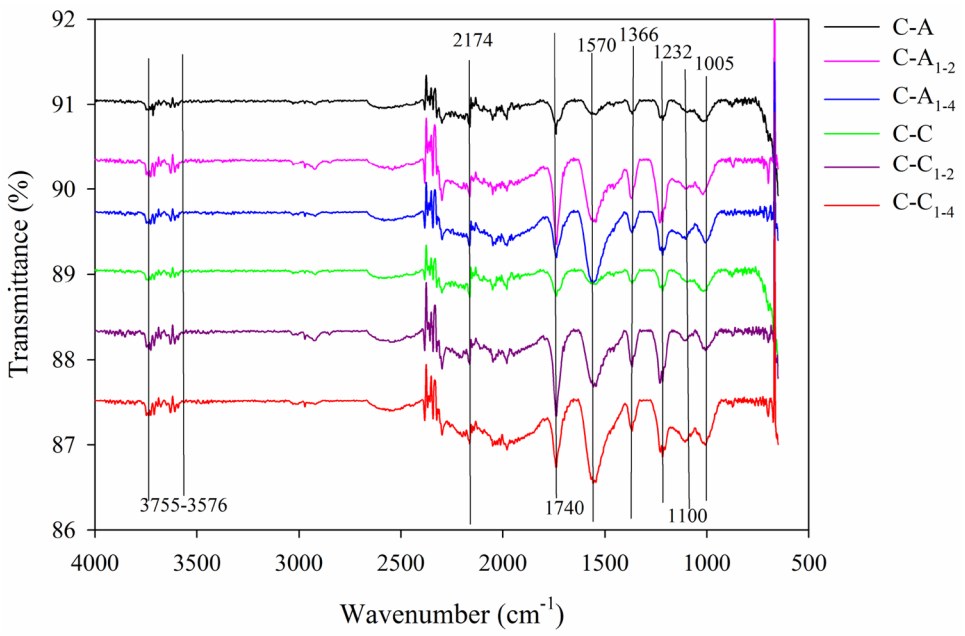

Fig. 6 FTIR spectra for the biochars obtained from the apple tree and cherry tree sawdust

groups depends on the precursor from which the biochars were obtained and on the activator content (KOH).

The point of zero charge (pH_{pzc}) determines the value of pH at which the net surface charge on the adsorbent equals zero [54, 78]. The value of pH_{pzc} determined for the tested materials from the graphs (Figs. 7, 8) is approx. 6.6–6.9 (Table 3) indicating that in the solution of $pH > pH_{pzc}$ the biochar surface has a negative charge while for $pH < pH_{pzc}$ the surface has a positive charge [54, 78]. The pH_{pzc} values are consistent with the results obtained by the Boehm's method (Table 3).

The thermal analysis was applied for estimation of the thermal stability of the materials. Figures 9 and 10 show the TG%, DTG and DTA curves for the biochars obtained from various organic precursors.

As follows from the analysis of the mass loss curves (TG%) the starting biochars are thermally stable only up to the temperature of ~ 300–400 °C and the complete thermal degradation of the carbon material is over in the temperature range of 800–1000 °C, depending on the organic material precursor. The KOH impregnation causes reduction in the thermal stability, the process of thermal degradation begins and ends at the temperatures lower than it is observed for the unmodified biochars. This is related to better development of porosity and surface functionalities due to the use of the activator. Moreover, activation with the use of KOH resulted in the carbon content decrease and significant oxygen content increase, which occur mainly in the form of surface functional groups in activated materials. These functionalities are a subject to desorption and thermal degradation much more easily than the ordered carbon structures, therefore the thermal stability of activated biochars is smaller. The analysis of the TG% = f (T) curves (Figs. 9, 10) shows that the type of organic precursor and the action of the activating agent affect the thermal stability.

Table 3 The biochars functional surface groups determined by the Boehm method and the pH_{pzc} values

Biochars	Total basic groups (mmol/g)	Total acidic groups (mmol/g)	Phenolic groups (mmol/g)	Lactone groups (mmol/g)	Carboxylic groups (mmol/g)	Carbonyl groups (mmol/g)	pH_{pzc}
$C–O_{1-2}$	0.68	1.53	0.62	0.37	0.25	0.29	6.67
$C–O_{1-4}$	0.69	1.74	0.68	0.44	0.25	0.37	6.62
$C–H_{1-2}$	1.06	1.17	0.50	0.50	0.12	0.05	6.61
$C–H_{1-4}$	1.12	1.56	1.12	0.13	0.25	0.06	6.53
$C–A_{1-2}$	1.19	1.62	0.87	0.38	0.25	0.12	6.88
$C–A_{1-4}$	1.06	2.11	1.00	0.25	0.50	0.36	6.25
$C–C_{1-2}$	0.94	1.50	0.59	0.47	0.34	0.10	6.33
$C–C_{1-4}$	1.06	1.76	0.26	0.56	0.50	0.44	6.62

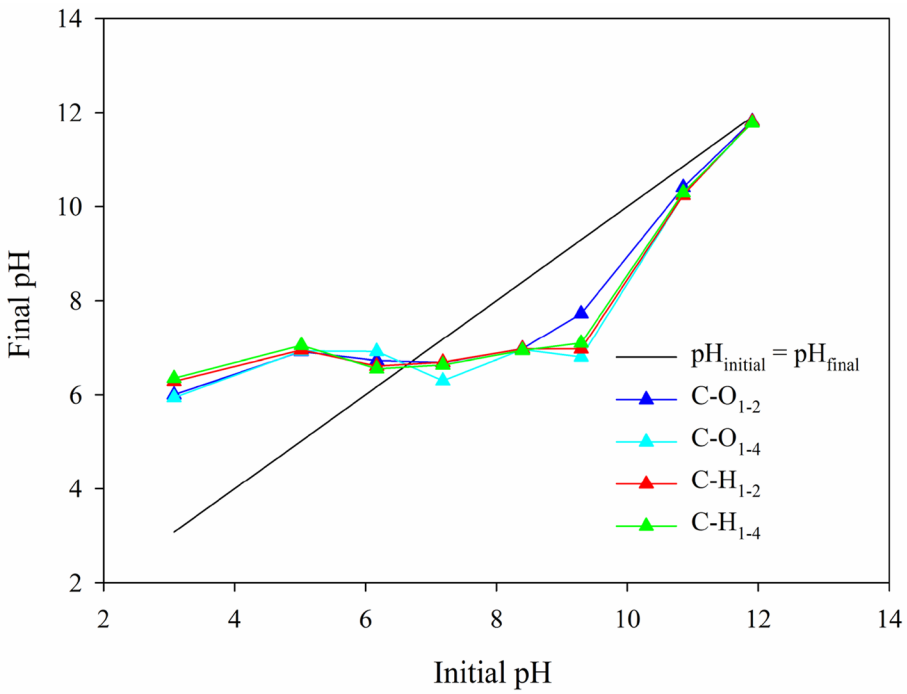

Fig. 7 Point of zero charge (pH_{pzc}) for the biochars obtained from the oak and hornbeam sawdust

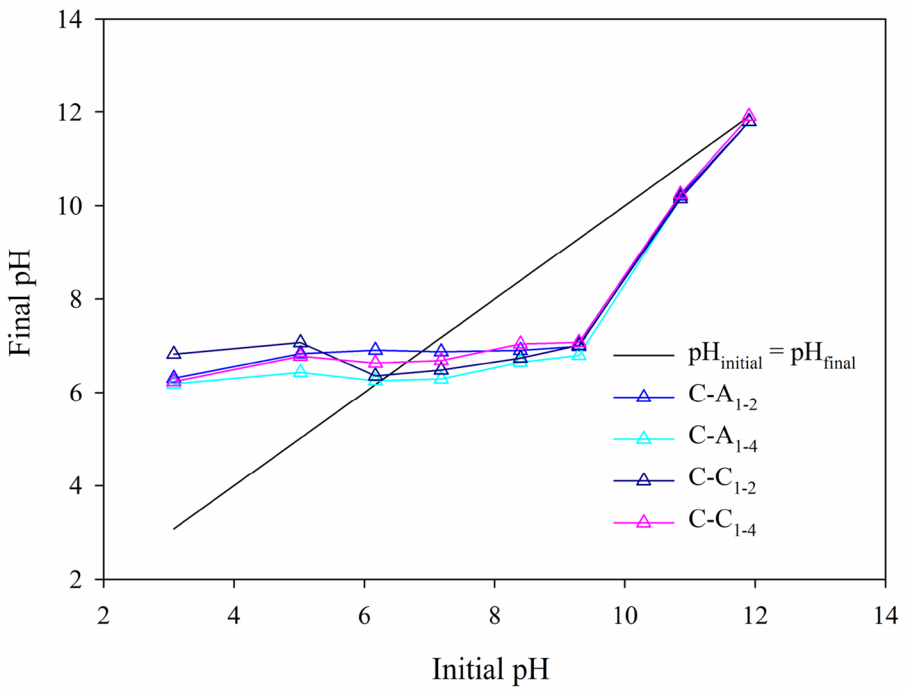

Fig. 8 Point of zero charge (pH_{pzc}) for the biochars obtained from the apple tree and cherry tree sawdust

On the basis of the TGA analysis performed in the atmosphere of O_2 and N_2, a proximate assessment of the type of carbon matter in the tested biocarbons was made. The results of research on the ash content, volatile and fixed carbon as well as the share of fixed carbon matter in the biocarbons are presented in Table 4.

According to data analysis in Table 4 the activation with the use of KOH changes the nature of the structure of the carbon material effectively. As the activation degree increased, the volatile matter (% VC) contents increased significantly, while the fixed carbon contents (% FC) decreased slightly in the biocarbons obtained from

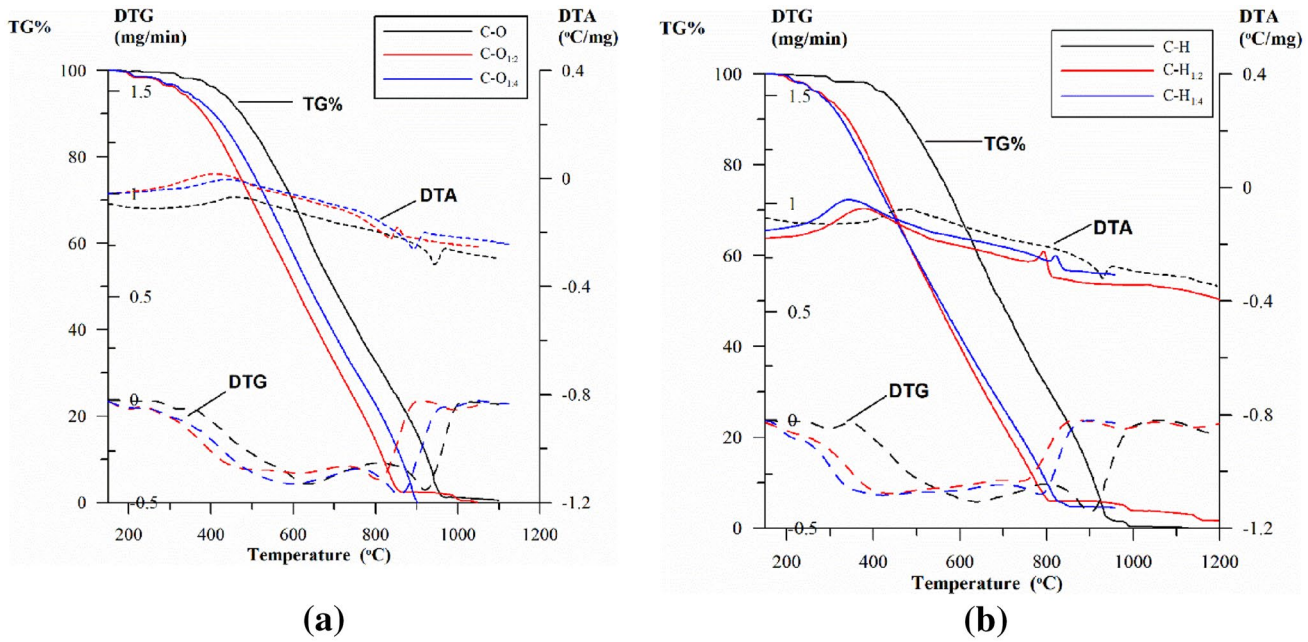

Fig. 9 TG%, DTG and DTA curves for the biochars based on the oak (**a**) and hornbeam (**b**) sawdust

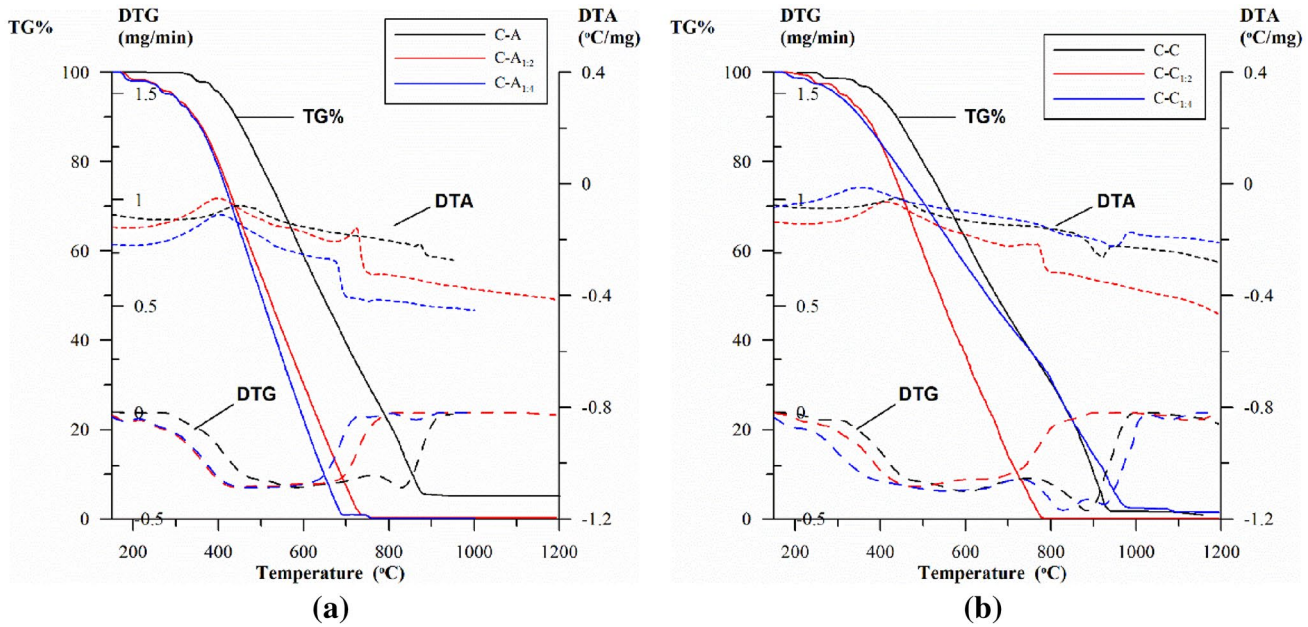

Fig. 10 TG%, DTG and DTA curves for the biochars obtained based on the apple tree (**a**) and cherry tree (**b**) sawdust

different biomass sources (Table 4). At the same time it was found that the share of the thermostable carbon matter (% C_{thermo}) in the starting biocarbons is very similar (~ 90%, Table 4) whereas the activation with an increasing amount of KOH causes a slight decrease in the share of the thermally stable fraction. This confirms that pyrolysis at the temperature of 800 °C is an effective method of obtaining stable biochars while the additional modification changes the materials structure effectively reducing their thermal stability.

Table 4 The proximate analysis and thermostability indices of biocarbons

Sample	%VC	%A	%FC	$\%C_{thermo}$
C–O	9.4	1.2	89.4	90.5
$C–O_{1-2}$	18.2	2.4	79.4	81.4
$C–O_{1-4}$	23.3	0.1	76.6	76.7
C–H	7.7	0.3	92.0	92.3
$C–H_{1-2}$	22.4	3.4	74.2	76.8
$C–H_{1-4}$	26.3	4.7	69.0	72.4
C–A	11.6	5.4	83.0	87.7
$C–A_{1-2}$	22.4	0.1	77.5	77.6
$C–A_{1-4}$	23.7	0.1	76.2	76.3
C–C	10.0	1.5	88.5	89.8
$C–C_{1-2}$	22.0	0.1	77.9	78.0
$C–C_{1-4}$	37.3	2.2	60.5	61.9

The results of pulse chemisorption and temperature-programmed desorption (TPD) of ammonia for the studied biochars are presented in Table 5. When analyzing the data of the pulse chemisorption of ammonia there was observed the following dependence: for all tested biochars, ammonia adsorption increases with the increasing temperature. The adsorption capacity of the obtained biochars depends on several factors: the carbon precursor, the degree of development of the porous structure and the size of the specific surface area. The developed microporous structure, and thus the large specific surface area (Table 1) play a key role in the process of ammonia adsorption on the tested adsorbents. The largest adsorption capacity was demonstrated for the $C\text{-}A_{1-4}$ material: 3.05 mmol/g (temperature 20 °C), the remaining biochars were characterized by a slightly smaller value of this parameter. The smallest adsorption capacity value was obtained for the material $C–H_{1-2}$: 2.24 mmol/g. The results of EDS, FTIR Boehm's titration and pH_{pzc} clearly show that the KOH activation causes oxidation of the surface and formation of oxygen functional groups in which those of strongly acidic character dominate. This has a positive effect on the ammonia chemisorption.

Based on results of the ammonia temperature programmed desorption TPD (Table 5) it was found that a very small amount of ammonia was desorbed although quite a large amount of this gas was adsorbed. The small NH_3 desorption is related to the dominant presence of acidic groups (which proves that it is chemisorbed on the acidic groups). However, such an effect is beneficial because the tested carbon materials can trap the toxic gas ammonia.

Table 6 summarizes the maximum sorption capacities of the tested biochars and other carbon materials in order to compare their adsorption capacity from the gas phase with respect to NH_3 based on the literature data. It was shown that the tested biochars are characterized by good adsorption properties.

4 Conclusions

The paper proves that sawdust is a cheap and good carbon precursor. Moreover, the activation with KOH enables preparation of adsorbents with very good structural parameters, large specific surface area and developed microporosity. After the activation process, the adsorbents were characterized by an ordered porous structure. The type of organic precursor and the action of the activator affect the thermal stability of the obtained biochar. The predominance of acidic and basic groups was observed on the surface of all tested biochars. It was proved that the obtained carbon adsorbents remove the harmful gas, which is ammonia, from the gas phase effectively. Moreover, very little of this gas is desorbed, so the resulting biochars can be promising as far as the trap of NH_3 and possibly of other toxic gases is concerned.

Table 5 The NH_3 adsorption capacity and TPD for the tested activated biochars

Biochars	NH_3 adsorption capacity (mmol/g) Pressure ~ 750 mmHg			TPD NH_3 (mmol/g) Pressure ~ 750 mmHg		
T (℃)	0	10	20	0–250	10–250	20–250
$C–O_{1-2}$	1.19	1.74	2.38	0.20	0.23	0.27
$C–O_{1-4}$	2.02	2.33	2.78	0.20	0.24	0.28
$C–H_{1-2}$	0.96	1.39	2.24	0.19	0.20	0.31
$C–H_{1-4}$	1.21	1.62	2.40	0.22	0.25	0.29
$C–A_{1-2}$	1.80	2.23	2.59	0.26	0.33	0.41
$C–A_{1-4}$	2.01	2.55	3.05	0.28	0.32	0.36
$C–C_{1-2}$	1.81	2.34	2.61	0.14	0.28	0.32
$C–C_{1-4}$	1.92	2.48	2.95	0.16	0.26	0.42

Table 6 The comparison of the maximal adsorption capacity in relation to NH_3 for the tested biochars with that of other carbon adsorbents

Carbon materials	S_{BET} (m^2/g)	Adsorption capacity (mmol/g)	Ref
OAK-250-KOH[a]	–	1.47	[7]
OAK-450-KOH[b]	–	0.35	[7]
AC[c]	430	0.78–4.19	[79]
AC[d]	450	0.77–5.08	[79]
AC[e]	1161	1.19	[80]
Na-OH-AC[f]	1125	1.69	[80]
HNO_3-AC[g]	1010	3.07	[80]
AA-WS250-AR[h]	851	3.11	[81]
BC-1-CO_2-6h[i]	1181	1.13–5.18	[6]
BC-2-CO_2-6h[i]	1167	0.95–3.95	[6]
C–O_{1-2}	714	1.19–2.38	This study
C–O_{1-4}	831	2.02–2.78	This study
C–H_{1-2}	672	0.96–2.24	This study
C–H_{1-4}	718	1.21–2.40	This study
C–A_{1-2}	775	1.80–2.59	This study
C–A_{1-4}	912	2.01–3.05	This study
C–C_{1-2}	788	1.81–2.61	This study
C–C_{1-4}	880	1.92–2.95	This study

[a]Hydrochar obtained from the oak wood, pyrolysis: 250 °C, activation: KOH

[b]Biochar obtained from the oak wood, pyrolysis: 450 °C, activation: KOH

[c]Activated carbon

[d]Activated carbon

[e]Active carbon pellets

[f]Active carbon impregnation: $NaNO_3$ in water, calcination: He, 773 K, 3 h

[g]Active carbons, activation: aqueous HNO_3, calcination: He, 773 K, 3 h

[h]Biochars from the wood shaving waste, pyrolysis: 250 °C, activation: 30% H_3PO_4 (450 °C/60 min)

[i]Biochar from the spruce cones, one-step or three-step pyrolysis in CO_2

Author contributions KJ performed the experiments, designed the conception, wrote the manuscript and discussed the results; BC performed the thermogravimetric measurements and prepared the discussion of results; final revision of the manuscript. All authors have read and agreed to the published version of the manuscript.

Funding This work was supported by Ministry of Education and Science, Poland (research project SUPB.RN.21.159).

Data availability Not applicable.

Declarations

Competing interests Nothing to declare.

Ethical approval Not applicable.

References

1. Břendová, K., Száková, J., Lhotka, M., Krulikovská, T., Punčochář, M., Tlustoš, P.: Biochar physicochemical parameters as a result of feedstock material and pyrolysis temperature: predictable for the fate of biochar in soil? Environ. Geochem. Health **39**, 1381–1395 (2017). https://doi.org/10.1007/s10653-017-0004-9
2. Galinato, S.P., Yoder, J.K., Granatstein, D.: The economic value of biochar in crop production and carbon sequestration. Energy Policy **39**, 6344–6350 (2011). https://doi.org/10.1016/j.enpol.2011.07.035
3. Wang, J., Wang, S.: Preparation, modification and environmental application of biochar: a review. J. Clean. Prod. **227**, 1002–1022 (2019). https://doi.org/10.1016/j.jclepro.2019.04.282
4. Lyu, H., Zhang, Q., Shen, B.: Application of biochar and its composites in catalysis. Chemosphere **240**, 124842–124852 (2020). https://doi.org/10.1016/j.chemosphere.2019.124842
5. Bamdad, H., Hawboldt, K., MacQuarrie, S.: A review on common adsorbents for acid gases removal: focus on biochar. Renew. Sustain. Energy Rev. **81**, 1705–1720 (2018). https://doi.org/10.1016/j.rser.2017.05.261
6. Jedynak, K., Charmas, B.: Preparation and characterization of physicochemical properties of spruce cone biochars activated by CO_2. Materials **14**, 3859–3875 (2021). https://doi.org/10.3390/ma14143859
7. Takaya, C.A., Parmar, K.R., Fletcher, L.A., Ross, A.B.: Biomass-derived carbonaceous adsorbents for trapping ammonia. Agriculture **9**, 16–30 (2019). https://doi.org/10.3390/agriculture9010016
8. Ndoun, M.C., Elliott, H.A., Preisendanz, H.E., Williams, C.F., Knopf, A., Watson, J.E.: Adsorption of pharmaceuticals from aqueous solutions using biochar derived from cotton gin waste and guayule bagasse. Biochar **3**, 89–104 (2021). https://doi.org/10.1007/s42773-020-00070-2
9. Praveen, S., Jegan, J., Pushpa, T.B., Gokulan, R., Bulgariu, L.: Biochar for removal of dyes in contaminated water: an overview. Biochar **4**, 10–25 (2022). https://doi.org/10.1007/s42773-022-00131-8
10. Ponnam, V., Katari, N.K., Mandapati, R.N., Nannapaneni, S., Tondepu, S., Jonnalagadda, S.B.: Efficacy of biochar in removal of organic pesticide, bentazone from watershed systems. J. Environ. Sci. Health B **55**, 396–405 (2020). https://doi.org/10.1080/03601234.2019.1707008
11. Kong, L.-L., Liu, W.-T., Zhou, Q.-X.: Biochar: an effective amendment for remediating contaminated soil. Rev. Environ. Contam. Toxicol. **228**, 83–99 (2013). https://doi.org/10.1007/978-3-319-01619-1_4
12. Waqas, M., Aburiazaiza, A.S., Miandad, R., Rehan, M., Barakat, M.A., Nizami, A.S.: Development of biochar as fuel and catalyst

in energy recovery technologies. J. Clean. Prod. **188**, 477–488 (2018). https://doi.org/10.1016/j.jclepro.2018.04.017
13. Cho, D.W., Kim, S., Tsang, Y.F., Song, H.: Preparation of nitrogen-doped Cu-biochar and its application into catalytic reduction of p-nitrophenol. Environ. Geochem. Health **41**, 1729–1737 (2019). https://doi.org/10.1007/s10653-017-9966-x
14. Tang, J., Zhu, W., Kookana, R., Katayama, A.: Characteristics of biochar and its application in remediation of contaminated soil. J. Biosci. Bioeng. **116**, 653–659 (2013). https://doi.org/10.1016/j.jbiosc.2013.05.035
15. Danish, M., Ahmad, T.: A review on utilization of wood biomass as a sustainable precursor for activated carbon production and application. Renew. Sustain. Energy Rev. **87**, 1–21 (2018). https://doi.org/10.1016/j.rser.2018.02.003
16. Vijayaraghavan, K., Balasubramanian, R.: Application of pinewood waste-derived biochar for the removal of nitrate and phosphate from single and binary solutions. Chemosphere **278**, 130361 (2021). https://doi.org/10.1016/j.chemosphere.2021.130361
17. Zhou, Y., Liu, X., Xiang, Y., Wang, P., Zhang, J., Zhang, F., Wei, J., Luo, L., Lei, M., Tang, L.: Modification of biochar derived from sawdust and its application in removal of tetracycline and copper from aqueous solution: adsorption mechanism and modelling. Biores. Technol. **245**, 266–273 (2017). https://doi.org/10.1016/j.biortech.2017.08.178
18. Nowicki, P., Kuszyńska, I., Przepiórski, J., Pietrzak, R.: The effect of chemical activation method on properties of activated carbons obtained from pine cones. Cent. Eur. J. Chem. **11**, 78–85 (2013). https://doi.org/10.2478/s11532-012-0140-0
19. Saletnik, B., Zaguła, G., Grabek-Lejko, D., Kasprzyk, I., Bajcar, M., Czernicka, M., Puchalski, C.: Biosorption of cadmium(II), lead(II) and cobalt(II) from aqueous solution by biochar from cones of larch (*Larix decidua* Mill. Subsp. decidua) and spruce (*Picea abies* L. H. Karst). Environ. Earth Sci. **76**, 574–584 (2017). https://doi.org/10.1007/s12665-017-6916-y
20. Sen, T.K., Afroze, S., Ang, H.M.: Equilibrium, kinetics and mechanism of removal of methylene blue from aqueous solution by adsorption onto pine cone biomass of *Pinus radiate*. Water Air Soil Pollut. **218**, 499–551 (2011). https://doi.org/10.1007/s11270-010-0663-y
21. Ahmad, M., Lee, S.S., Dou, X., Mohan, D., Sung, J., Yang, J.E., Ok, Y.S.: Effects of pyrolysis temperature on soybean stover and peanut shell-derived biochar properties and TCE adsorption in water. Biores. Technol. **118**, 536–544 (2012). https://doi.org/10.1016/j.biortech.2012.05.042
22. Tomul, A., Arslan, Y., Kabak, B., Trak, D., Kendüzler, E., Lima, E.C., Tran, H.N.: Peanut shells-derived biochars prepared from different carbonization processes: Comparison of characterization and mechanism of naproxen adsorption in water. Sci. Total Environ **726**, 137828 (2020). https://doi.org/10.1016/j.scitotenv.2020.137828
23. Fawzy, S., Osman, A.I., Farrell, C., Al-Muhtaseb, A.H., Harrison, J., Al-Fatesh, A.S., Fakeeha, A.H., Doran, J., Yang, H., Rooney, D.W.: Characterization and kinetic modeling for pyrolytic conversion of cotton stalks. Energy Sci. Eng. **9**, 1908–1918 (2021). https://doi.org/10.1002/ese3.961
24. Assirey, E.A., Altamimi, L.R.: Chemical analysis of corn cob-based biochar and its role as water decontaminants. J. Taibah Univ. Sci. **15**, 111–121 (2021). https://doi.org/10.1080/16583655.2021.1876350
25. Mari Selvam, S., Janakiraman, T., Paramasivan, B.: Characterization of engineered corn cob biochar produced in allothermal pyrolysis reactor. Mater. Today Proc. **47**, 312–317 (2021). https://doi.org/10.1016/j.matpr.2021.04.469
26. Zhang, K., Sun, P., Faye, M.C.A.S., Zhang, Y.: Characterization of biochar derived from rice husks and its potential in chlorobenzene degradation. Carbon **130**, 730–740 (2018). https://doi.org/10.1016/j.carbon.2018.01.036
27. Zhang, P., O'Connor, D., Wang, Y., Jiang, L., Xia, T., Wang, L., Tsang, D.C.W., Ok, Y.S., Hou, D.: A green biochar/iron oxide composite for methylene blue removal. J. Hazard. Mater. **384**, 121286–121293 (2020). https://doi.org/10.1016/j.jhazmat.2019.121286
28. Zięzio, M., Charmas, B., Jedynak, K., Hawryluk, M., Kucio, K.: Preparation and characterization of activated carbons obtained from the waste materials impregnated with phosphoric acid(V). App. Nanosci. **10**(12), 4703–4716 (2020). https://doi.org/10.1007/s13204-020-01419-6
29. Liu, C., Yin, Z., Hu, D., Mo, F., Chu, R., Zhu, L., Hu, C.: Biochar derived from chicken manure as a green adsorbent for naphthalene removal. Environ. Sci. Pollut. Res. **28**, 36585–36597 (2021). https://doi.org/10.1007/s11356-021-13286-x
30. Xu, X., Hu, X., Ding, Z., Cheng, Y., Gao, B.: Waste-art-paper biochar as an effective sorbent for recovery of aqueous Pb(II) into value-added PbO nanoparticles. Chem. Eng. J **308**, 863–871 (2017). https://doi.org/10.1016/j.cej.2016.09.122
31. Mazlan, M.A.F., Uemura, Y., Yusup, S., Elhassan, F., Uddin, A., Hiwada, A., Demiya, M.: Activated carbon from rubber wood sawdust by carbon dioxide activation. Procedia Eng. **148**, 530–537 (2016). https://doi.org/10.1016/j.proeng.2016.06.549
32. Khalili, S., Khoshandam, B., Jahanshahi, M.: A comparative study of CO_2 and CH_4 adsorption using activated carbon prepared from pine cone by phosphoric acid activation. Korean J. Chem. Eng. **33**, 2943–2952 (2016). https://doi.org/10.1007/s11814-016-0138-y
33. Oginni, O., Singh, K., Oporto, G., Dawson-Andoh, B., McDonald, L., Sabolsky, E.: Influence of one-step and two-step KOH activation on activated carbon characteristics. Bioresour. Technol. Rep. **7**, 100266–100275 (2019). https://doi.org/10.1016/j.biteb.2019.100307
34. Sivakumar, P., Palanisamy, P.N.: Adsorption studies of Basic Red 29 by a non-conventional activated carbon prepared from Euphorbia antiquorum L. Int. J. ChemTech Res. **1**, 502–510 (2009)
35. Ding, S., Liu, Y.: Adsorption of CO_2 from flue gas by novel seaweed-based KOH-activated porous biochars. Fuel **260**, 116382–116391 (2020). https://doi.org/10.1016/j.fuel.2019.116382
36. Hui, T.S., Zaini, M.A.A.: Potassium hydroxide activation of activated carbon: a commentary. Carbon Lett. **16**, 275–280 (2015). https://doi.org/10.5714/CL.2015.16.4.275
37. Ahmadpour, A., Do, D.D.: The preparation of active carbons from coal by chemical and physical activation. Carbon **34**, 471–479 (1996). https://doi.org/10.1016/0008-6223(95)00204-9
38. Jagtoyen, M., Thwaites, M., Stencel, J., McEnaney, B., Derbyshire, F.: Adsorbent carbon synthesis from coals by phosphoric acid activation. Carbon **30**, 1089–1096 (1992). https://doi.org/10.1016/0008-6223(92)90140-R
39. Zhu, X.-L., Wang, P.-Y., Peng, C., Yang, J., Yan, X.-B.: Activated carbon produced from paulownia sawdust for high-performance CO_2 sorbents. Chin. Chem. Lett. **25**, 929–932 (2014). https://doi.org/10.1016/j.cclet.2014.03.039
40. Yang, L., Feng, Y., Cao, M., Yao, J.: Two-step preparation of hierarchical porous carbon from KOH-activated wood sawdust for supercapacitor. Mater. Chem. Phys. **238**, 121956–121962 (2019). https://doi.org/10.1016/j.matchemphys.2019.121956
41. Quan, C., Su, R., Gao, N.: Preparation of activated biomass carbon from pine sawdust for supercapacitor and CO_2 capture. Int. J. Energy Res. **44**, 1–17 (2020). https://doi.org/10.1002/er.5206
42. Liu, L., Jin, S., Park, Y.P.Y.C., Lee, C.-H.: Sorption equilibria and kinetics of CO_2, N_2, and H_2O on KOH-treated activated carbon. Ind. Eng. Chem. Res. **57**, 17218–17225 (2018). https://doi.org/10.1021/acs.iecr.8b03862
43. Marques, S.C.R., Mestre, A.S., Machuqueiro, M., Gotvajn, A.Ž, Marinšek, M., Carvalho, A.P.: Apple tree branches derived

activated carbons for the removal of β-blocker atenolol. Chem. Eng. J. **345**, 669–678 (2018). https://doi.org/10.1016/j.cej.2018.01.076
44. Elmouwahidi, A., Bailón-García, E., Pérez-Cadenas, A.F., Maldonado-Hódar, F.J., Carrasco-Marín, F.: Activated carbons from KOH and H_3PO_4-activation of olive residues and its application as supercapacitor electrodes. Electrochim. Acta **229**, 219–228 (2017). https://doi.org/10.1016/j.electacta.2017.01.152
45. Borhan, A., Taha, M.F., Hamzah, A.A.: Characterization of activated carbon from wood sawdust prepared via chemical activation using potassium hydroxide. Adv. Mater. Res. **832**, 132–137 (2014). https://doi.org/10.4028/www.scientific.net/AMR.832.132
46. Huang, C.C., Li, H.S., Chen, C.H.: Effect of surface acidic oxides of activated carbon on adsorption of ammonia. J. Hazard. Mater. **159**, 523–527 (2008). https://doi.org/10.1016/j.jhazmat.2008.02.051
47. Rodrigues, C.C., Moraes, D., Jr., Nóbrega, S.W., Barboza, M.G.: Ammonia adsorption in a fixed bed of activated carbon. Biores. Technol. **98**, 886–891 (2007). https://doi.org/10.1016/j.biortech.2006.03.024
48. Gonçalves, M., Sánchez-García, L., Oliveira-Jardim, E., Silvestre-Albero, J., Rodríguez-Reinoso, F.: Ammonia removal using activated carbons: effect of the surface chemistry in dry and moist conditions. Environ. Sci. Technol. **45**, 10605–10610 (2011). https://doi.org/10.1021/es203093v
49. Yeom, C., Kim, Y.: Adsorption of ammonia using mesoporous alumina prepared by a templating method. Environ. Eng. Res. **22**, 401–406 (2017). https://doi.org/10.4491/eer.2017.045
50. Chen, Y., Li, L., Li, J., Ouyang, K., Yang, J.: Ammonia capture and flexible transformation of M-2(INA) (M=Cu Co, Ni, Cd) series materials. J. Hazard. Mater. **306**, 340–347 (2016). https://doi.org/10.1016/j.jhazmat.2015.12.046
51. Rezaei, E., Schlageter, B., Nemati, M., Predicala, B.: Evaluation of metal oxide nanoparticles for adsorption of gas phase ammonia. J. Environ. Chem. Eng. **5**, 422–431 (2017). https://doi.org/10.1016/j.jece.2016.12.026
52. Boehm, H.P.: Some aspects of the surface chemistry of carbon blacks and other carbons. Carbon **32**, 759–769 (1994)
53. Boehm, H.P.: Surface oxides on carbon and their analysis: a critical assessment. Carbon **40**, 145–149 (2002)
54. Lim, C.K., Bay, H.H., Noeh, C.H., Aris, A., Majid, Z.A., Ibrahim, Z.: Application of zeolite-activated carbon macrocomposite for the adsorption of Acid Orange 7: isotherm. Kinetic and thermodynamic studies. Environ. Sci. Pollut. Res. **20**, 7243–7255 (2013). https://doi.org/10.1007/s11356-013-1725-7
55. Rivera-Utrilla, J., Bautista-Toledo, I., Ferro-García, M.A., Moreno-Castilla, C.: Activated carbon surface modifications by ad-sorption of bacteria and their effect on aqueous lead adsorption. J. Chem. Technol. Biotechnol. **76**, 1209–1215 (2001). https://doi.org/10.1002/jctb.506
56. Calvelo Pereira, R., Kaal, J., Camps Arbestain, M., Pardo Lorenzo, R., Aitkenhead, W., Hedley, M., Macías, F., Hindmarsh, J., Maciá-Agulló, J.A.: Contribution to characterisation of biochar to estimate the labile fraction of carbon. Org. Geochem. **42**, 1331–1342 (2011). https://doi.org/10.1016/j.orggeochem.2011.09.002
57. Cárdenas-Aguiar, E., Gascó, G., Paz-Ferreiro, J., Méndez, A.: Thermogravimetric analysis and carbon stability of chars produced from slow pyrolysis and hydrothermal carbonization of manure waste. J. Anal. Appl. Pyrol. **140**, 434–443 (2019). https://doi.org/10.1016/j.jaap.2019.04.026
58. Brunauer, S., Emmett, P.H., Teller, E.: Adsorption of gases in multimolecular layers. J. Am. Chem. Soc. **60**, 309–319 (1938)
59. Kruk, M., Jaroniec, M.: Gas adsorption characterization of ordered organic-inorganic nanocomposite materials. Chem. Mater. **13**, 3169–3183 (2001). https://doi.org/10.1021/cm0101069
60. Jagiello, J., Olivier, J.P.: 2D-NLDFT adsorption models for carbon slit-shaped pores with surface energetical heterogeneity and geometrical corrugation. Carbon **55**, 70–80 (2013). https://doi.org/10.1016/j.carbon.2012.12.011
61. Jagiello, J., Olivier, J.P.: Carbon slit pore model incorporating surface energetical heterogeneity and geometrical corrugation. Adsorption **19**, 777–783 (2013). https://doi.org/10.1007/s10450-013-9517-4
62. Sing, K.S.W., Everett, D.H., Haul, R.A.W., Moscou, L., Pierotti, R.A., Rouquerol, J., Siemieniewska, T.: Reporting physisorption data for gas/solid systems with special reference to the determination of surface area and porosity. Pure Appl. Chem. **57**, 603–619 (1985)
63. Yang, H.M., Zhang, D.H., Chen, Y., Ran, M.J., Gu, J.C.: Study on the application of KOH to produce activated carbon to realize the utilization of distiller's grains. IOP Conf. Ser. Earth Environ. Sci. **69**, 012051 (2017). https://doi.org/10.1088/1755-1315/69/1/012051
64. Januszewicz, K., Kazimierski, P., Klein, M., Kardaś, D., Łuczak, J.: Activated carbon produced by pyrolysis of waste and wood and straw for potential wastewater adsorption. Materials **13**, 2047–2059 (2020). https://doi.org/10.3390/ma13092047
65. Wang, J., Kaskel, S.: KOH activation of carbon-based materials for energy storage. J. Mater. Chem. **22**, 23710–23725 (2012). https://doi.org/10.1039/c2jm34066f
66. Yang, H., Wang, Y., Liu, Z., Liang, D., Liu, F., Zhang, W., Di, X., Wang, C., Ho, S.-H., Chen, W.-H.: Enhanced thermal conductivity of waste sawdust-based composite phase change materials with expanded graphite for thermal energy storage. Bioresour. Bioprocess. **4**, 1–12 (2017). https://doi.org/10.1186/s40643-017-0182-4
67. Yao, Y., Gao, B., Inyang, M., Zimmerman, A.R., Cao, X., Pullammanappallil, P., Yang, L.: Biochar derived from anaerobically digested sugar beet tailings: characterization and phosphate removal potential. Biores. Technol. **102**, 6273–6278 (2011). https://doi.org/10.1016/j.biortech.2011.03.006
68. Ofomaja, A.E., Naidoo, E.B.: Biosorption of copper from aqueous solution by chemically activated pine cone: a kinetic study. Chem. Eng. J. **175**, 260–270 (2011). https://doi.org/10.1016/j.cej.2011.09.103
69. Si, X., Lu, F., Chen, J., Lu, R., Huang, Q., Jiang, H., Taarning, E., Xu, J.: A strategy for generating high-quality cellulose and lignin simultaneously from woody biomass. Green Chem. **19**, 4849–4857 (2017). https://doi.org/10.1039/c7gc02492d
70. Ma, R., Ma, Y., Gao, Y., Cao, J.: Preparation of micro mesoporous carbon from seawater impregnated sawdust by low temperature one step CO_2 activation for adsorption of oxytetracycline. SN Appl. Sci. **2**, 171–185 (2020). https://doi.org/10.1007/s42452-020-1940-z
71. Marciniak, M., Goscianska, J., Pietrzak, R.: Physicochemical characterization of ordered mesoporous carbons functionalized by wet oxidation. J. Mater. Sci. **53**, 5997–6007 (2018). https://doi.org/10.1007/s10853-017-1960-2
72. Vaughn, S.F., Kenar, J.A., Thompson, A.R., Peterson, S.C.: Comparison of biochars derived from wood pellets and pelletized wheat straw as replacements for peat in potting substrates. Ind. Crops. Prod. **51**, 437–443 (2013). https://doi.org/10.1016/j.indcrop.2013.10.010
73. Garnuszek, M., Szczepanik, B., Gawinkowski, S., Słomkiewicz, P.M., Witkiewicz, Z., Jedynak, K.: Spectral characterization of mesoporous carbons modified by Ag, Au, TiO_2 and Fe_3O_4 nanoparticles. Ochr. Sr. **34**, 17–22 (2012). (**in Polish**)
74. Kim, D.J., Lee, H.I., Yie, J.E., Kim, S.-J., Kim, J.M.: Ordered mesoporous carbons: implication of surface chemistry, pore structure and adsorption of methyl mercaptan. Carbon **43**, 1868–1873 (2005). https://doi.org/10.1016/j.carbon.2005.02.035

75. Emrooz, H.B.M., Maleki, M., Rashidi, A., Shokouhimehr, M.: Adsorption mechanism of a cationic dye on a biomass-derived microand mesoporous carbon: structural, kinetic, and equilibrium insight. Biomass Convers. Biorefin. **11**, 943–954 (2021). https://doi.org/10.1007/s13399-019-00584-1
76. Figueiredo, J.L., Pereira, M.F.R., Freitas, M.M.A., Órfao, J.J.M.: Modification of the surface chemistry of activated carbons. Carbon **37**, 1379–1389 (1999). https://doi.org/10.1016/S0008-6223(98)00333-9
77. Putra, E.K., Pranowo, R., Sunarso, J., Indraswati, N., Ismadji, S.: Performance of activated carbon and bentonite for adsorption of amoxicillin from wastewater: mechanisms, isotherms and kinetics. Water Res. **43**, 2419–2430 (2009). https://doi.org/10.1016/j.watres.2009.02.039
78. Al-Degs, Y.S., El-Barghouthi, M.I., El-Sheikh, A.H., Walker, G.M.: Effect of solution pH, ionic strength, and temperature on adsorption behavior of reactive dyes on activated carbon. Dyes Pigm. **77**, 16–23 (2008). https://doi.org/10.1016/j.dyepig.2007.03.001
79. Helminen, J., Helenius, J., Paatero, E., Turunen, I.: Adsorption equilibria of ammonia gas on inorganic and organic sorbents at 298.15 K. J. Chem. Eng. Data **46**, 391–399 (2001). https://doi.org/10.1021/je000273+
80. Liu, C.Y., Aika, K.: Effect of surface oxidation of active carbon on ammonia adsorption. Bull. Chem. Soc. Jpn. **76**, 1463–1468 (2003). https://doi.org/10.1246/bcsj.76.1463
81. Ro, K.S., Lima, I.M., Reddy, G.B., Jackson, M.A., Gao, B.: Removing gaseous NH_3 using biochar as an adsorbent. Agriculture **5**, 991–1002 (2015). https://doi.org/10.3390/agriculture5040991